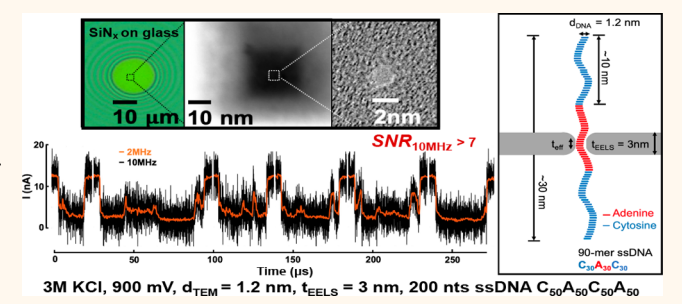
Single-Stranded DNA Translocation Recordings through Solid-State Nanopores on Glass Chips at 10 MHz Measurement **Bandwidth**

Chen-Chi Chien, Siddharth Shekar, David J. Niedzwiecki, Kenneth L. Shepard, and Marija Drndić*, To

Supporting Information

Downloaded via UNIV OF PENNSYLVANIA on February 17, 2020 at 05:15:01 (UTC). See https://pubs.acs.org/sharingguidelines for options on how to legitimately share published articles.

ABSTRACT: Accurate and low-cost analysis of biomolecules is important for many applications. This work seeks to further improve the measurement bandwidths achievable with solid-state nanopores, which have emerged as an important platform for this analysis. We report singlestranded DNA translocation recordings at a bandwidth of 10 MHz copolymers of 80 ($C_{20}A_{20}C_{20}A_{20}$), 90 ($C_{30}A_{30}C_{30}$), and 200 (C₅₀A₅₀C₅₀A₅₀) nucleotides through Si nanopores with effective diameters of 1.4-2.1 nm and effective membrane thicknesses 0.5-8.9 nm. By optimizing glass chips with thin nanopores and by integrating them with



custom-designed amplifiers based on complementary metal-oxide-semiconductor technology, this work demonstrates detection of translocation events as brief as 100 ns with a signal-to-noise ratio exceeding seven at a measurement bandwidth of 10 MHz. We also report data robustness and variability across 13 pores of similar size and thickness, yielding a current blockade between 30 and 60% with a mean ionic current blockade (ΔI) of $\sim 3-9$ nA and a characteristic dwell time of $\sim 2-21$ ns per nucleotide. These measurements show that characteristic translocation rates are at least 10 times faster than previously recorded. We detect transient intraevent fluctuations, multiple current levels within translocation events, and variability of DNA translocation event signatures and durations.

KEYWORDS: low capacitance glass chips, solid-state nanopores, low-noise amplifier, DNA, silicon nitride, DNA sequencing

anopores are emerging as a versatile platform for studying various biomolecules, such as DNA, providing single-molecule detection, high-throughput, and real-time feedback. In the case of DNA sequencing, nanopores offer the promise of long read lengths and reduced cost. 1-10 Successful nanopore systems for DNA sequencing to date are based on tracking the real-time operation of enzymes operating on a strand of DNA through protein nanopores. In this context, MspA pores in lipid bilayer membranes with ratcheting polymerases have been used to sequence individual DNA nucleotides.4

Solid-state nanopore platforms offer an alternative to protein pores, delivering higher signal levels, diameter tunability, and stability. These higher signal levels translate into the ability to achieve better temporal resolution when coupled to optimized electronics, 6-10 which we address in this work. Higher temporal resolution holds the promise of enzymeless, freerunning nanopore sequencing when sufficient bandwidth performance can be achieved and if the entropy associated with the DNA motion during translocation can be controlled and reduced. This also benefits enzyme-ratcheting approaches by reducing error rates associated with the temporal stochasticity of enzyme dynamics.

Use of optimized complementary metal-oxide-semiconductor (CMOS) transimpedance amplifiers has previously been shown to yield faster nanopore recordings. 7,8 In such highbandwidth measurements, the overall capacitance of the chip, amplifier, and wiring combine with the input-referred voltage noise of the amplifier to determine the total input-referred

Received: June 13, 2019 Accepted: August 26, 2019 Published: August 26, 2019

[†]Department of Physics and Astronomy, University of Pennsylvania, Philadelphia, Pennsylvania 19104, United States

[‡]Department of Electrical Engineering, Columbia University, New York, New York 10027, United States

[§]Goeppert LLC, Pennovation Works, 3401 Grays Ferry Avenue, Philadelphia, Pennsylvania 19146, United States

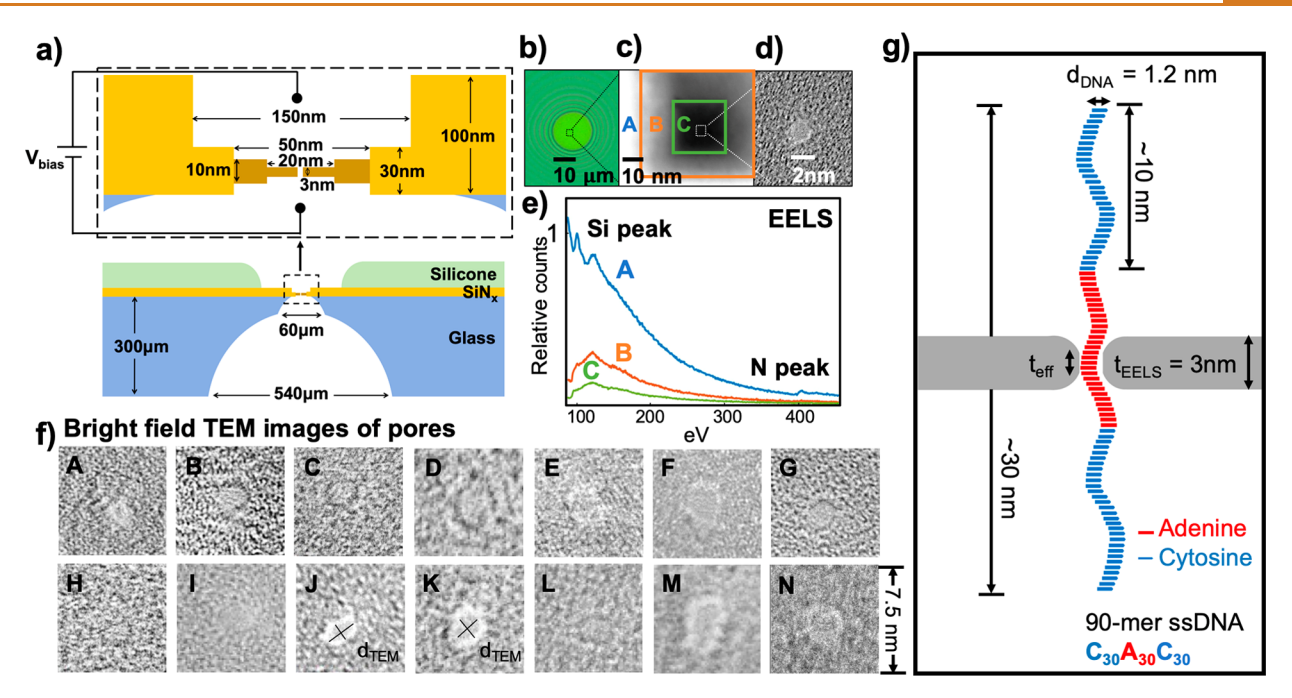


Figure 1. Glass (fused-silica) chips with small and thin solid-state pores. (a) Schematics of the measurement setup and cross-sectional view of the glass chip and the solid-state pore. (b) Circular, $20 \,\mu\mathrm{m}$ diameter, suspended SiN_x window on top of a fused-silica (glass) substrate. (c) High-angle annular dark-field image of thin a-Si/SiO₂ membrane geometry. Labeled "A" is the area that was thinned down to 30 nm by reactive ion etching. Labeled "B" is the area that was thinned using scanning TEM techniques down to ~10 nm. ²⁴ Labeled "C" is the area of the second thinning step, where we thin down the membrane to 3–8 nm, calibrated by electron energy loss spectroscopy (EELS). (d) Brightfield (BF) image of a nanopore that is drilled in the thinnest region C in part (c). (e) EELS spectrum of the respective region in part (c). The N peak is completely depleted when a nanopore is drilled. The Si peak is used to monitor the thickness of the thin membrane. Region C has roughly 0.1 relative counts with respect to region A, translating to 3 nm thickness. ²⁴ (f) BF images of nanopores measured in this work. The TEM diameter (d_{TEM}) is measured as shown as examples in Pore J and Pore K of elliptical and circular pores. (g) Schematics of single-stranded DNA translocation through a nanopore shown to scale with the dimension specified.

current noise. Decreasing either of these components helps reduce the overall noise in the recordings. For DNA detection, nanopore diameters, similar to single-stranded DNA (ssDNA) cross-sectional size (~1.2 nm), and thin pores, approaching atomic levels comparable to nucleotide spacing (\sim 0.3 nm), are optimal. 9-15 Although there is no consensus on the rate of free-running DNA translocation through nanopores, estimated by dividing the total translocation time by the number of nucleotides, speeds of >10 nt/ μ s have been reported for silicon-based nanopores with similar experimental conditions of buffered KCl solutions, pore diameters <2 nm, pore thicknesses <5 nm, and bias voltages up to 1 V.7,8,16 The translocation speed has traditionally been reduced by choosing higher viscosity solutions, heavier ions, or by lowering the solution's temperature, at the cost of slowing down detection and limiting the size of detectable molecules. 8,9,16-

In this article, we report data from ssDNA translocation recordings from 13 pores at measurement bandwidths up to 10 MHz. Each pore records $\sim 10^2$ events per second, and at 10 MHz bandwidth, we detect events and features within an event as short as 100 ns. This capability is achieved by combining custom-designed CMOS amplifiers, glass (fused-silica) chips with SiN_x membranes with sub-1 to 2 pF capacitance, and 1.4 to 2.1 nm effective-diameter Si pores with an effective thickness of 0.5–8.9 nm. Although previous work focused on optimizing the chip^{20–23} or the amplifier^{6,7} separately, optimization of all experimental parts simultaneously (amplifier, membrane, interconnects) is necessary to achieve the results presented here. The membrane capacitance and input capacitance of the amplifier are comparable in our study. We

measure time traces of the ionic current for ssDNA from 80 to 200 nucleotides (nt) in length—poly(dA)₂₀poly(dC)₂₀poly(dA)₂₀poly(dC)₂₀, poly(dC)₃₀poly(dA)₃₀poly(dC)₃₀, and poly(dA)₅₀poly(dC)₅₀poly(dA)₅₀poly(dC)₅₀. The 20 to 50 nt long homopolymer segments used here have lengths of 6–15 nm (nucleotide separation is ~0.3 nm), designed to be comparable or longer than the pore thicknesses. Pores were drilled in amorphous silicon/SiO_x membranes produced from a local, multistep thinning of silicon nitride (SiN_x) membranes by reactive ion etching, followed by focused electron beam etching in the scanning transmission electron microscope. We report events with signal-to-noise ratios over seven at 10 MHz with event durations as short as 100 ns.

RESULTS AND DISCUSSION

Figure 1a shows a representative cross section of the nanopores studied in this work. When a bias voltage is applied across two electrolyte solution chambers separated by a dielectric membrane containing a nanopore, ssDNA is driven through the nanopore, blocking the baseline ionic current. This current block can be measured by a low-noise amplifier. To make small diameter and thin pores within low-capacitance membranes, we fabricate fused-silica (glass) substrates (Figure 1a) instead of using a conventional silicon substrate to suspend the silicon nitride membrane. These 300 μ m thick glass chips were especially designed for high-bandwidth experiments to reduce the chip capacitance below 1 pF, 21-23 exposing a circular region of the silicon nitride membrane with a diameter of 10–30 μ m (Figure 1b). A 30 nm thick, 150 × 150 nm² region is then produced in this silicon nitride membrane with electron-

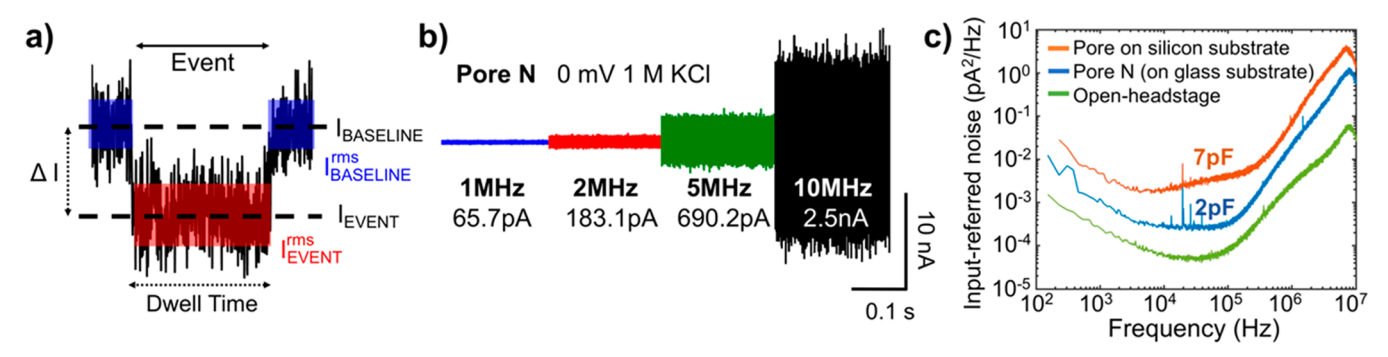


Figure 2. Translocation event parameters, noise, and noise comparison of glass and silicon chips. (a) Schematic of a typical event of ssDNA translocation through a nanopore, taken from Pore F, with important parameters labeled. I_{BASELINE} and I_{EVENT} are taken to be the mean value. The blue box represents the noise in the baseline, $I_{\text{EVENT}}^{\text{ms}}$, and the red box represents the noise within the event $I_{\text{EVENT}}^{\text{ms}}$. (b) Concatenated time trace of a 20 ms long, 0 mV baseline measurement of Pore N. Each section corresponds to the same trace filtered using a digital four-pole Bessel filter to cutoff frequencies of 1, 2, and 5 MHz. The 10 MHz trace has no extra filtering except the effect of an analogue four-pole Bessel filter while recording. Corresponding $I_{\text{BASELINE}}^{\text{ms}}$ values are shown below the filtering frequency. (c) Input-referred current noise (power spectral density (PSD)) for the open headstage configuration of the amplifier (green), PSD for pore N on the glass chip (blue), and the PSD for a pore on the silicon chip from Shekar *et al.* (orange) with measured chip capacitances of 2 and 7 pF, respectively.

beam lithography and reactive ion etching. Finally, pore diameters and thicknesses were optimized for ssDNA measurements using a thinning and drilling procedure developed previously on Si substrates. 7,24 The 200 keV focused electron beam was rastered within a 50 × 50 nm² region at high beam current until the thickness decreased from ~30 to 10 nm. We then scanned over a smaller region of $20 \times 20 \text{ nm}^2$ with a slightly lower beam current to ensure precise control of the thickness to as thin as 1 nm (Figure 1c).²⁴ Molecular dynamics simulations performed previously showed that amorphous silicon membranes can be stable down to thicknesses of 0.7nm, ²⁴ consistent with our observations. The adjustment of the transmission electron microscopy (TEM) beam current is achieved by changing the condenser lens and apertures. The pore is drilled at the thinnest area by holding the beam position fixed at a desired spot for a few seconds, resulting in pores <2 nm in diameter, as shown in Figure 1d. The narrow nanopores allow only single-file ssDNA translocation, as the nanopore diameter is only ~0.2-0.9 nm wider than ssDNA.

Figure 1e shows the whole scanning TEM (STEM) thinning process where membrane thickness is monitored and calibrated simultaneously from the electron energy loss spectroscopy (EELS) spectrum. Due to charging on these glass chips, the beam could move slightly, requiring manual correction of the beam's position. Because of the lighter atomic weight of N (=14) compared to that of Si (=28) atoms, the rate of N atoms being sputtered is faster, resulting in an amorphous silicon membrane by the time it reaches the desired thickness of several nanometers. The EELS spectrum shows that, at this stopping thickness, there is no more N peak at ~400 eV. The atoms are sputtered from the top and from the bottom, resulting in a double-sided, trench-like pore geometry best depicted by Figure 1a. The amorphous silicon is known to naturally oxidize after exposure to air after being taken out of the TEM chamber, resulting in the membrane turning into a-Si/SiO_x; the nanopore shape and size were checked subsequently and remained unchanged in TEM images after the pores were exposed to air and imaging was repeated. Figure 1f shows the TEM bright-field images of nanopores used here, labeled from A to N. The image contrast is weak because the membranes are locally only about 1 nm thick, comparable to the thickness of 2D materials and in

contrast to the typical image contrast of thicker SiN_x pores.²⁴ Figure 1g shows an illustration to scale of a 90 nt $poly(dC)_{30}poly(dA)_{30}poly(dC)_{30}$ ssDNA translocating through a pore with dimensions comparable to those used in this study.

Figure 2a summarizes the relevant signal and noise levels of a typical translocation event. Before and after the event, the average ionic current in the open-pore state is denoted as $I_{\rm BASELINE}$. The noise in this baseline current, $I_{\rm BASELINE}^{\rm rms}$, is the root-mean-square input-referred current noise of the open-pore signal in the absence of translocating DNA. $I_{\rm EVENT}$ is defined as the mean current value during an event with $\Delta I = I_{\rm BASELINE} - I_{\rm EVENT}$. The rms current noise within an event is denoted by $I_{\rm EVENT}^{\rm rms}$.

In order to observe small changes in the ionic current, increasing signal-to-noise ratio (SNR) is important. We define SNR as $\Delta I/I_{\rm BASELINE}^{\rm rms}$. At sufficiently high bandwidths, $I_{\rm BASELINE}^{\rm rms}$ is given by the equation $I_{\rm BASELINE}^{\rm rms}(B) = \left(\frac{2\pi}{\sqrt{3}}\right)B^{3/2}C\nu_n^{25}$ where B is the bandwidth of measurement, ν_n is the input-referred voltage noise of the amplifier, and C is the total capacitance at the input of the amplifier and typically consists of the chip capacitance, $C_{\rm chip}$, the wiring capacitance, $C_{\rm w}$, and the capacitance of the amplifier, $C_{\rm amp}$. Improvements in SNR can be obtained by decreasing $I_{\rm BASELINE}^{\rm rms}$ and increasing ΔI .

To estimate $I_{\rm BASELINE}$, we use a simple cylindrical resistor model²⁶ of the pore surrounded by the top and bottom ionic hemispheres (access regions), where $R_{\rm pore} = \frac{4t_{\rm eff}}{\sigma\pi d_{\rm eff}^2}$, and including the contribution of the access regions, $R_{\rm access} = \frac{1}{2\sigma d_{\rm eff}}$, resulting in

$$I_{\text{BASELINE}} = V_{\text{bias}} \sigma \left(\frac{4t_{\text{eff}}}{\pi d_{\text{eff}}^2} + \frac{1}{d_{\text{eff}}} \right)^{-1}$$
(1)

where σ is the conductivity of solution, $t_{\rm eff}$ is the effective nanopore thickness, and $d_{\rm eff}$ is the effective nanopore diameter. The current blocked by DNA translocating through the pore can be estimated by

Table 1. Summary and Comparison of the Recent High-Bandwidth DNA Translocation Recordings at 1 MHz and Higher Bandwidth

| year/reference | 2012 Rosenstein. et al.6 | 2015 Balan et al. ²¹ | 2016 Shekar et al. ⁷ | 2019 this work |
|--|-----------------------------------|---------------------------------|------------------------------------|------------------------------------|
| pore material | SiN_x | SiN_x | a-Si/SiO _{x} | a-Si/SiO _{x} |
| substrate material | silicon | fused silica | silicon | fused silica |
| pore thickness | 10 nm | 100 nm | ~3 nm | ~3 nm |
| pore diameter | 4 nm | 4 nm | <2 nm | <2 nm |
| $ u_{ m n}$ | $5.3 \text{ nV}/\sqrt{\text{Hz}}$ | $1 \text{ nV}/\sqrt{\text{Hz}}$ | $3.15 \text{ nV}/\sqrt{\text{Hz}}$ | $3.15 \text{ nV}/\sqrt{\text{Hz}}$ |
| C_{amp} | 2.15 pF | 20 pF | 4 pF | ~3.25 pF |
| $C_{ m pore}$ | 6 pF | 1 pF | ~10 pF | 1-2 pF |
| ΣC | 8.15 pF | 21 pF | 14 pF | 4-5 pF |
| highest bandwidth of translocations reported | 1 MHz (dsDNA) | 1 MHz (dsDNA) | 5 MHz (ssDNA) | 10 MHz (ssDNA) |
| input-referred noise at 1 MHz bandwidth | 155 pA rms | 110 pA rms | 128 nA rms | 65 nA rms |

Table 2. Summary of Nanopore Parameters and Translocation Statistics Extracted from Data from All 13 a-Si/SiO_x Nanopores^a

| pore | d _{TEM} (nm) | $d_{ m eff} (m nm)$ | $t_{ m EELS} \ m (nm)$ | $t_{ m eff} \ (m nm)$ | voltage (mV) | KCl (M) | $	au_{	ext{dwell}} (\mu 	ext{s})$ | $I_{ m BASELINE} \ m (nA)$ | $\langle \Delta I \rangle$ (nA) | $\langle \Delta I angle / I_{ m BASELINE}$ | ⟨ <i>G</i> ⟩ (nS) | $\langle \Delta G \rangle$ (nS) | ssDNA (nts) | rate (ns/ nt) |
|------|-----------------------|----------------------|-------------------------|------------------------|-----------------|------------|-----------------------------------|-----------------------------|---------------------------------|---|----------------------|---------------------------------|----------------|------------------|
| A | 0.9 | 1.5 | 3 | 8.9 | 900 | 3 | 1.2 | 4.8 | 3.0 | 0.62 | 5.4 | 3.3 | 200 | 5.8 |
| В | 1.2 | 1.5 | 3 | 3.6 | 900 | 3 | 3.0 | 10.6 | 6.1 | 0.58 | 11.7 | 6.8 | 200 | 14.8 |
| C | 1.6×2 | 1.4 | 3 | 0.5 | 500 | 3 | 0.8 | 14.8 | 8.5 | 0.58 | 29.6 | 17.0 | 200 | 4.2 |
| D | 1.8×2.4 | 1.4* | 3 | 0* | 400 | 3 | 0.5 | 18.1 | 9.0 | 0.50 | 45.2 | 22.5 | 200 | 2.3 |
| E | 1.8 | 1.7 | 3 | 3.3 | 900 | 3 | 1.0 | 13.1 | 6.2 | 0.47 | 14.6 | 6.9 | 80 | 13.1 |
| F | 1.8 | 1.7 | 3 | 2.6 | 900 | 3 | 2.0 | 15.8 | 7.1 | 0.45 | 17.6 | 7.9 | 200 | 10.0 |
| G | 1.6 | 1.9 | 3 | 4.2 | 900 | 3 | 1.5 | 13.4 | 5.6 | 0.43 | 14.8 | 6.2 | 90 | 16.3 |
| H | 1.7 | 1.7 | 3 | 2.1 | 900 | 3 | 1.1 | 19.0 | 7.9 | 0.42 | 21.1 | 8.8 | 200 | 5.4 |
| I | 1.8 | 1.7 | 5 | 0.9 | 900 | 1 | 1.4 | 10.8 | 4.1 | 0.38 | 12.0 | 4.6 | 90 | 15.6 |
| J | 1.2×1.7 | 2.0 | 8 | 2.3 | 700 | 3 | 0.8 | 17.1 | 5.3 | 0.31 | 24.4 | 7.6 | 90 | 9.1 |
| K | 1.7 | 2.0 | 8 | 1.9 | 700 | 3 | 0.5 | 19.0 | 5.8 | 0.31 | 27.1 | 8.3 | 90 | 5.3 |
| L | 1.6 | 2.1 | 3 | 2.3 | 900 | 1 | 0.7 | 9.2 | 2.6 | 0.28 | 10.2 | 2.8 | 90 | 7.9 |
| M | 1.4×2.2 | 1.7 | 5 | 1.5 | 900 | 1 | 1.9 | 8.7 | 3.5 | 0.27 | 9.6 | 3.9 | 90 | 20.9 |

"Measured at room temperature with filtering at 2 MHz using an "8 σ threshold" to define events. d_{TEM} is measured from TEM images as illustrated in Figure 1f. t_{EELS} is the thickness measured from the EELS spectrum. d_{eff} and t_{eff} are the effective diameters and thicknesses calculated using a simple cylindrical model for nanopore conductance (eqs 1 and 2). τ_{dwell} are the characteristic dwell times for ssDNA molecules obtained by fitting the event time histograms by an exponential function, and rates are the characteristic dwell times divided by the number of nucleotides. For the 13 pores we presented here, the baseline current increased within 10% of the starting open-pore current within a 10 min time interval. *Note that for Pore D, the calculated t_{eff} is negative, and we set t_{eff} to be 0 to obtain an approximate d_{eff} value.

$$\Delta I = \sigma V_{\text{bias}} \left[\left[\frac{4t_{\text{eff}}}{\pi d_{\text{eff}}^2} + \frac{1}{d_{\text{eff}}} \right]^{-1} - \left[\frac{4t_{\text{eff}}}{\pi (d_{\text{eff}}^2 - d_{\text{DNA}}^2)} + \frac{1}{\sqrt{d_{\text{eff}}^2 - d_{\text{DNA}}^2}} \right]^{-1} \right]$$
(2)

where $V_{\rm bias}$ is the applied transmembrane voltage and $d_{\rm DNA}$ is the cross-sectional width of ssDNA. The signal, $\Delta I_{\rm r}$ is maximized when the pore diameter approaches the width of DNA and when the nanopore thickness is minimized.

Translocation rates of single-stranded DNA molecules through solid-state nanopores with parameters similar to those in this work have been reported to be as fast as 1 μ s/nt, with studies suggesting significantly faster rates of up to 100 ns/nt.^{7,8,16} It is important to note that these per nucleotide translocation rates are rough estimates from the total translocation times measured, using strong assumptions of uniform translocation speeds, and that the start and end of events correspond to DNA entering and leaving the pore. These time scales suggest that single-nucleotide detection will require a measurement bandwidth of at least 10 MHz.

Our measurement hardware performs anti-alias filtering at 10 MHz and samples the data at 40 million samples per second (MSps). We further filter the data to lower bandwidths as required, using a digital approximation of a fourth-order lowpass Bessel filter. We also filter some of the data sets with wavelet filters, which have been shown to improve SNR based on the pulse-like nature of the signal waveforms.²⁷ Nanopores on low-capacitance glass chips with SiN, membranes are integrated with a CMOS amplifier with an input capacitance of 3.25 pF, v_n of 3.15 nV/ $\sqrt{\text{Hz}}$, and a maximum recording bandwidth of 10 MHz. Figure 2b shows the integrated inputreferred noise for Pore N, $d_{\text{TEM}} = 1.6 \text{ nm}$ and $t_{\text{EELS}} = 3 \text{ nm}$, measured in 1 M KCl, $I_{\text{BASELINE}}^{\text{rms}}$ is 65.7 pA_{rms}, 183.1 pA_{rms}, $690.2~pA_{rms}$, and $2.5~nA_{rms}$ at 1, 2, 5, and 10 MHz, respectively. Figure 2c shows the power spectral density of the open headstage of the amplifier, the noise spectrum for Pore N, and, for comparison, the best previous results obtained using the same amplifier using nanopores on membranes lacking the glass passivation described above. The reduced capacitance provided by the glass chips reduces the noise power across the entire frequency range by more than a factor of 2. At the full 10 MHz bandwidth, the integrated noise decreases by 40%, from 4.2 to 2.5 nA_{rms}. Table 1 quantifies the improvements

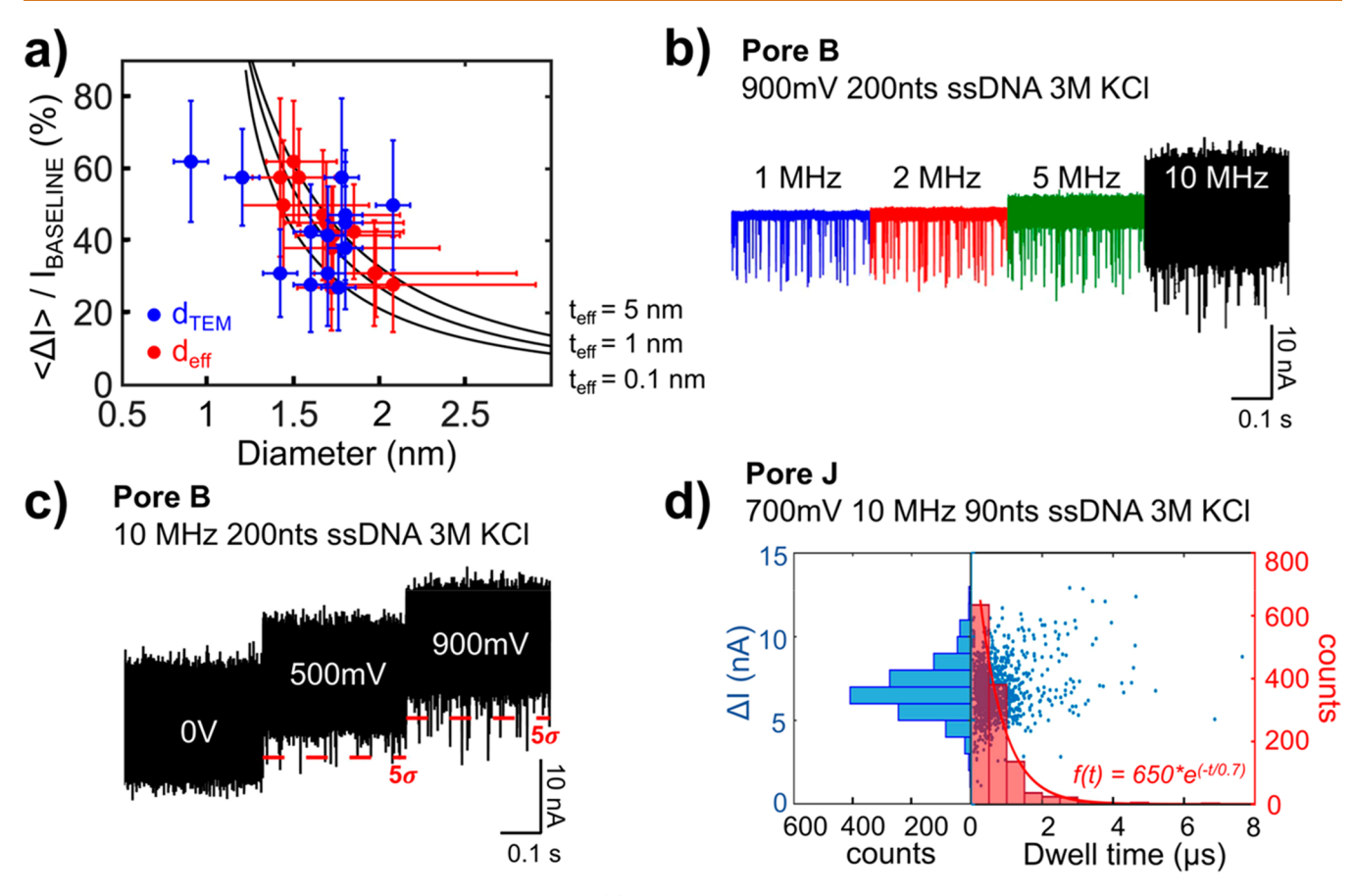


Figure 3. ssDNA translocation data analysis up to 10 MHz. (a) Percent of $\langle \Delta I \rangle/I_{\rm BASELINE}$ plotted as a function of the nanopore diameter, where red circles are $d_{\rm eff}$ and the blue circles are $d_{\rm TEM}$. The solid lines are calculated using a cylindrical model for effective thickness of 5, 1, and 0.1 nm. (b) Concatenated time traces of 0.4 s long recordings of 200 nt ssDNA through Pore B at 900 mV bias. The traces are filtered using a four-pole Bessel filter to 1, 2, and 5 MHz bandwidths, and also shown are the 10 MHz unfiltered data. All data recorded at 40 MSps. (c) Concatenated time trace of 200 nt ssDNA translocation recordings 10 MHz through Pore B at bias voltages of 0, 500, and 900 mV. The dotted red line is the 5σ threshold used to define detectable events. There are many events surpassing the 5σ threshold at as low as 500 mV bias voltage. (d) Dwell time vs amplitude scatter plot (points) and histograms (bars) of ~1000 translocation events at 10 MHz frequency of 90 nt ssDNA through Pore J at 700 mV bias voltage. The red curve represents an exponential fit to the dwell time histogram.

demonstrated in this work by comparing these data with previous high-bandwidth measurement efforts.

We performed short ssDNA translocation experiments with these glass chips containing a-Si/SiO $_x$ nanopores with TEM-measured diameters from 0.9 to 2.4 nm, Pores A–M. The bright-field TEM images of the pores are shown in Figure 1f. Membrane thicknesses from 3 to 8 nm were measured by EELS. Hardward Experiments were performed in buffered salt solutions of 1 or 3 M KCl at pH 8, a measured conductance of 11.8 S/m for 1 M and 30.6 S/m for 3 M, and transmembrane bias voltages up to 900 mV. Ionic current time traces for a fixed voltage were measured for 10 min periods or longer after introduction of 1 μ L of 200 nM ssDNA to the solution. At 40 MSps and with 12-bit quantization, data are generated at a rate of 60 MB/s, presenting challenges for real-time nanopore data analysis. We split the data into several one-second-long segments for subsequent analysis.

Table 2 shows results at a 2-MHz filter bandwidth, sorted in the order of decreasing average current blocked percentage, $\langle \Delta I \rangle / I_{\rm BASELINE}$. For these 13 pores, the pore diameter measured from TEM images $(d_{\rm TEM})$ ranges from 0.9 to 2.4 nm, whereas the membrane thickness determined from EELS $(t_{\rm EELS})$ varies from 3 to 8 nm. $\langle \Delta I \rangle / I_{\rm BASELINE}$ is as high as \sim 60%. We calculate an effective diameter $(d_{\rm eff})$ and effective

thickness ($t_{\rm eff}$) from the measured open-pore current $I_{\rm BASELINE}$ and the current blockade ΔI using the cylindrical model for nanopore conductance described previously. Figure 3a and Table 2 summarize the results of our analysis. The error bars in Figure 3a for $d_{\rm eff}$ and $t_{\rm eff}$ originate from the variance in ΔI , which propagates through the calculations. Figure 3a shows the blockade percentage $\langle \Delta I \rangle / I_{\rm BASELINE}$ as a function of $d_{\rm eff}$ and $d_{\rm TEM}$, as red and blue circles, respectively. For pores that are not circular (for example, Pore J in Figure 1f), $d_{\rm TEM}$ is approximated by taking the area of the pore and calculating a diameter of a circle with the same area. The solid black lines are the calculated blockade percentages as a function of $d_{\rm eff}$ for $t_{\rm eff} = 5$, 1, and 0.1 nm.

There is a small difference between $d_{\rm TEM}$ and $d_{\rm eff}$ up to ± 0.6 nm (Table 2). This difference can be attributed to several factors, including the fact that some of our pores are not perfectly circular, that their shapes and dimensions can change slightly after being taken out of the vacuum and immersed into the aqueous salt solution, and that the $d_{\rm eff}$ calculation does not consider the charge on the pore wall. Across all the pores used in this study, the estimated $d_{\rm eff}=1.4-2.1$ nm and $t_{\rm eff}=0-8.9$ nm. Note that for Pore D, the calculated $t_{\rm eff}$ is negative, and we set its $t_{\rm eff}$ to be 0 to obtain an approximate $d_{\rm eff}$ value. Pore clogging can happen during measurements. However, we

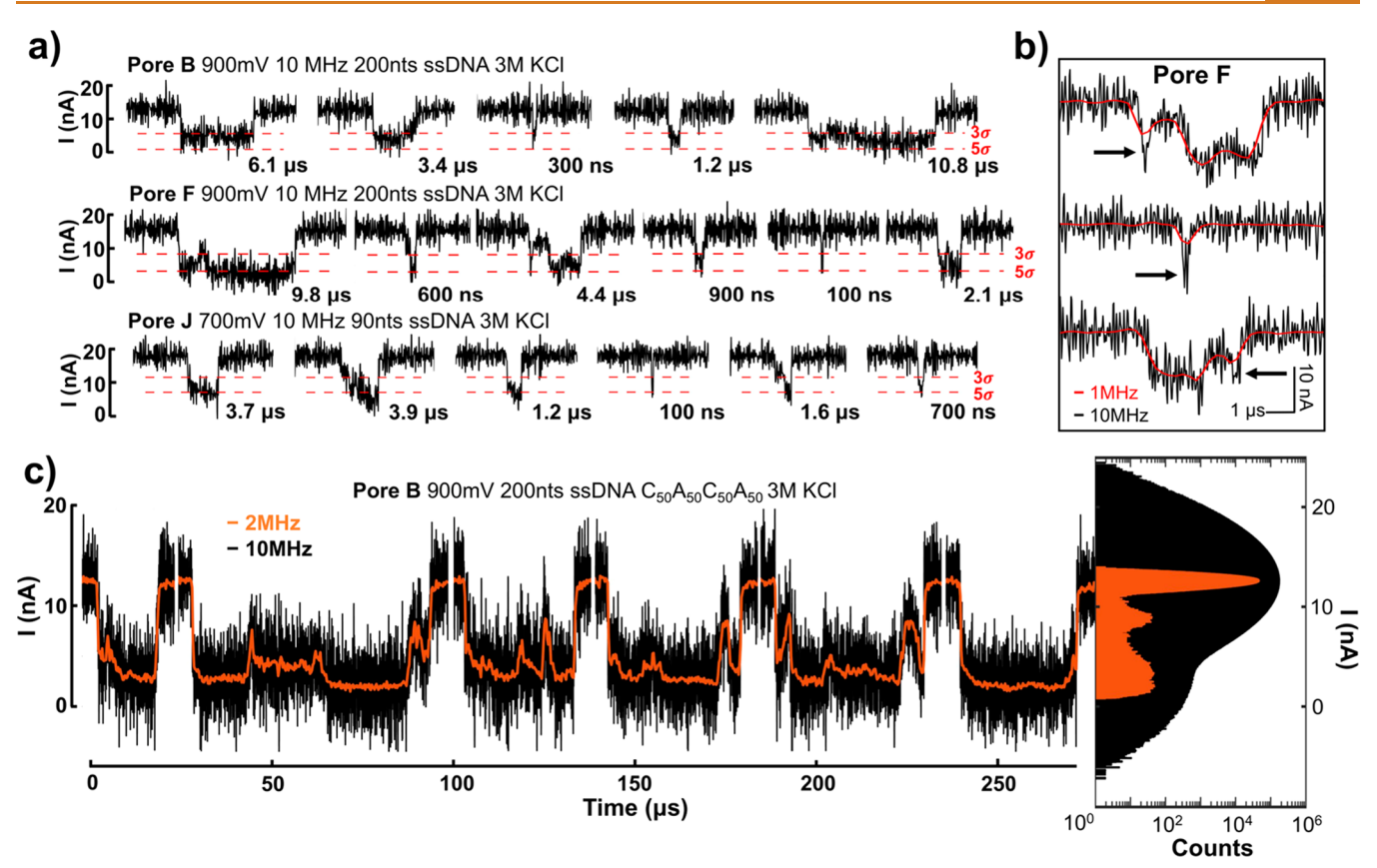


Figure 4. ssDNA translocation events at 10 MHz measurement bandwidth and comparison with data filtered at 1 and 2 MHz. (a) Sample events of unfiltered 10 MHz data containing translocation events of various durations from several pores (pore B, pore F, and pore J) and conditions as indicated. The events are as short as 100 ns. Only the events that surpass the 5σ thresholds are shown here, and the 3σ and 5σ threshold lines are marked by the red dashed lines. (b) Example events from pore F demonstrating short events and short features within the events that are missed or greatly attenuated in magnitude, indicated by arrows, at 1 MHz (red), but detectable at 10 MHz (black). (c) Concatenated traces of selected events with dwell times over $10 \,\mu s$ from pore B at bandwidths of $10 \, \text{MHz}$ (black) and 2 MHz (orange) are shown in the left panel. The right panel is the all-points histograms of a 1 s long current trace with 155 events from which 6 selected events to the left are chosen. The black histogram is for the data taken at 10 MHz, and the orange histogram is for the same data set but filtered down to 2 MHz.

prevent clogging by applying a voltage of opposite polarity. This reversed voltage repels the DNA from the pore, and the baseline current returns to its original open-pore current value. We observed that clogging happens at a frequency of roughly once per minute. The increase of the open-pore current during the measurement was also observed. For example, Pore F exhibited an increase of open-pore current, *I*, from 15.9 to 16.7 nA within the first 2 min of the measurements at 900 mV in 3 M KCl. This translates to a 5% increase in baseline current and an increase of about 0.05 nm in pore diameter, assuming an unchanged pore thickness.

One of the benefits of using solid-state pores is the ability to apply bias voltages higher than those in protein pore systems, increasing current signal levels and enabling high-bandwidth measurements. The higher noise in high-bandwidth measurements requires us to drive the voltage as high as 900 mV to have sufficient signal-to-noise to detect individual events. Event recognition is performed with simple thresholding at multiples of $\sigma = I_{\rm BASELINE}^{\rm ms}$, and we chose thresholding of $S\sigma$ to reduce false events at 10 MHz (see Section 1 in the Supporting Information). Nanopores here record only electrical signals, and there is no direct visualization of how exactly the DNA passes through the pore. However, when ssDNA goes through the pore under these conditions, it

typically blocks the amount of current close to what is calculated from the simple resistor model, and such events can be attributed to translocations.²⁴ For example, if the DNA blocks the pore completely, the current blockade should be 100%. On the other hand, when the blockade of the current is much smaller, this means that the DNA has either not gone through the pore or that the DNA has passed through the pore so quickly that we observe artificially attenuated current due to the lack of time resolution by the experimental setup. Such shallow current blockades are not included in the analysis as we have chosen the threshold to be 5σ of the baseline signal for 10 MHz data and 8σ of the baseline signal for 2 MHz data. Therefore, most events recorded have a measured value very close to the predicted value when DNA blocks the pore (see Table 2) and are therefore consistent with the fact that they correspond to DNA passage through the pore. For the smallest pore (Pore A), we achieve an average $\Delta I/I_{\rm BASELINE}$ over 60%, which corresponds well to the ssDNA width of 1.2 nm translocating through a nanopore of diameter 1.4 nm. A simple geometrical estimate based on the ratio of ssDNA-to-nanopore cross-sectional areas yields a comparable value of $1.2^2/1.4^2 \sim$

Figure 3b shows current time traces for Pore B at 1, 2, and 5 MHz and 10 MHz bandwidths, with ssDNA translocation

events clearly distinguishable at 10 MHz. Figure 3c shows time traces at 0 V, 500 mV, and 900 mV biases at 10 MHz from the same pore. The 5σ current levels are indicated in Figure 3c as red dotted lines. Only events with durations longer than 100 ns and less than 100 μ s are considered true events. The upper bound serves to exclude long events that we hypothesize correspond to situations when ssDNA molecules get stuck in the pore. These comprise on average \sim 7% of the total number of events, and the highest percentage, up to ~20%, is observed for the smallest pores, $d_{\rm eff} \sim 1.4$ nm. Smaller diameter pores and longer analytes, in general, should result in higher percentages of longer events, and we observe a weak correlation within the range of our diameters. (1.4-2.1 nm) and DNA lengths (80-200 nt) (see Section 2 in the Supporting Information). The lower bound for event duration detection is set to be twice the rise time of the four-pole Bessel filter. The four-pole Bessel filter has a rise time associated with the cutoff frequency chosen, with the rise time at 10 MHz being about 50 ns. Events shorter than twice this time would be attenuated in the current magnitude and temporally distorted and are not considered here. Therefore, we do not record events shorter than 100 ns because we cannot resolve them due to the limit of our setup. The scatter plot of 1251 events over the 5σ threshold at 10 MHz bandwidth from Pore I and the corresponding histogram of dwell time and event depth are plotted in Figure 3d for an applied voltage of 700 mV. The characteristic dwell time au_{dwell} is calculated by fitting the dwell time distribution to the exponential function $Ae_{\text{dwell}}^{-t/\tau}$ as shown as the red curve in the right panel.¹⁷ The fit equation for the dwell time is $f(t) = 650 \times e^{(-t/0.7)}$, and the *R*-square value is 0.98, indicating an appropriate fit. At the same 5σ threshold, the number of events recorded per second at 10 MHz bandwidth is smaller than the number of events recorded from the same traces filtered to lower bandwidth because of the increase in noise with bandwidth and the corresponding decrease of SNR. For example, Pore J produces approximately 1850 events at 2 MHz compared to 1251 events at 10 MHz over the same 3 s measurement window. Increasing the filtering bandwidth from 2 to 10 MHz increases $\langle \Delta I \rangle$ from 3.1 to 6.8 nA, as fewer small amplitude events are captured, and decreases the characteristic dwell time from 1.1 to 0.7 μ s (see Section 3 in the Supporting Information). At 10 MHz, we record current changes more accurately without attenuation for shorter events, detect short events that would have been missed at lower bandwidths, and have a higher temporal resolution for the events detected.

For pores with the highest SNRs, we resolve translocation events at 10 MHz. Figure 4a shows representative translocation events from Pore B, Pore F, and Pore J with durations as short as 100 ns. In Figure 4b, for comparison, we show some representative events also filtered to 1 MHz bandwidth; the 10 MHz bandwidth is clearly required to resolve many of the events detected. In particular, the transient current features at 10 MHz, indicated by arrows, are highly attenuated at 1 MHz.

In Figure 4c, we show concatenated traces of selected events of 200 nt poly(dA)₅₀poly(dC)₅₀poly(dC)₅₀poly(dC)₅₀ from Pore B that have durations between 10 and 100 μ s at both 10 and 2 MHz bandwidths. For Pore B, 38% of events have a dwell time between 10 and 100 μ s. We also observe structure within these events. Some events maintain fairly constant current values within the event, whereas others show switching levels and bumps (see Section 4 in the Supporting Information). A few recent studies claimed identification of

homopolymer blocks with solid-state nanopores. Goto et al. fabricated 5 nm thick SiN nanopores with calculated diameters down to 2 nm and showed that, in CsCl solution, triblock DNA copolymers, poly(dA)₅₄poly(dC)₃₃poly(dT)₃₃ and poly-(dG)₃₃poly(dA)₅₄poly(dT)₃₃, exhibit trimodal distributions in all-point histograms. 28 They attributed these peaks to signals from homopolymer blocks. This identification was made in the histograms showing current distributions but not within translocation events. We note that peaks in histograms are not sufficient proof of homopolymer block differentiation. For example, in Figure 4c, whereas we also observe a two-level allpoints histogram corresponding to two current levels visible within the events on the left, this apparent two-level structure in the individual events does not correspond to the number or order of homopolymer blocks, nor is it consistent from event to event. Yamazaki et al. claimed poly(dA) and poly(dC) detection within the same DNA strand with a ~1.4 nm diameter SiN nanopore with an effective thickness ~1.8 nm, as calculated from the pore current, by observing two distinct current levels in selected events comprising ~19% of total number of recorded events.²⁹ The signal was attributed to the unzipping of dsDNA through the nanopore with the calculated diameter smaller than the dsDNA diameter, and the two current levels were attributed to differences in the helical secondary structure of poly(dA) and poly(dC). Here, unfortunately, there are no consistent current levels that can be visually attributed to homopolymer segments, even when the data are denoised using wavelets (see Sections 5 and 6 in the Supporting Information). In the all-point histograms shown in Figure 4c, when we filter to 2 MHz to reduce the baseline noise, we observe several distinct peaks in the current distributions, suggesting these transient current features within an event could reflect movements and reorientations of ssDNA above and inside the pores, 30,31 but more modeling work is needed to understand their origin.³¹

To quantify the transient fluctuations, we calculate the magnitude of current fluctuations due to the presence of ssDNA in and around the pore as $I_{\text{DNA}}^{\text{rms}}$ $\sqrt{\left(I_{\mathrm{EVENT}}^{\mathrm{rms}}\right)^2 - \left(I_{\mathrm{BASELINE}}^{\mathrm{rms}}\right)^2}$. If one assumes a ΔI between adenine (A) and cytosine (C) of ~1 nA,8 one would expect current fluctuation due to this size difference in our segmented 90 nt $poly(dC)_{30}poly(dA)_{30}poly(dC)_{30}$ ssDNA homopolymer translocation events to be approximately 0.5 nA_{rms} (see Section 7 in the Supporting Information). Instead we find $I_{\text{DNA}}^{\text{rms}}$ on the order of 1.5 nA_{rms}, suggesting that these fluctuations reflect more than just nucleotide differences. For pores where the diameter is comparable to thickness, the access resistance is comparable to the resistance of the pore itself.²⁸ Across the 13 pores measured, $R_{\text{pore}}/(2R_{\text{access}})$ ranges from 0.5 to 7.5, where R_{pore} ranges from 10 to 160 M Ω . For smaller values of this ratio, the change of R_{access} by the presence of the DNA also contributes to the measured translation event. 6,7,24,30,31 The entropy of the ssDNA also contributes to I_{DNA}^{rms} and obfuscates more sequence-determined current traces. ssDNA entropy exceeds that of dsDNA, the more common analyte in previous solid-state nanopore studies, due to the much shorter persistence length of ssDNA compared to that of dsDNA.³² As illustrated in Figure 1g, the ssDNA outside the pores can possess various configurations and movements in the access region that will contribute to $I_{\text{DNA}}^{\text{rms}}$.

To evaluate whether a temporal resolution of 100 ns is sufficient to resolve the DNA sequence at the translocation

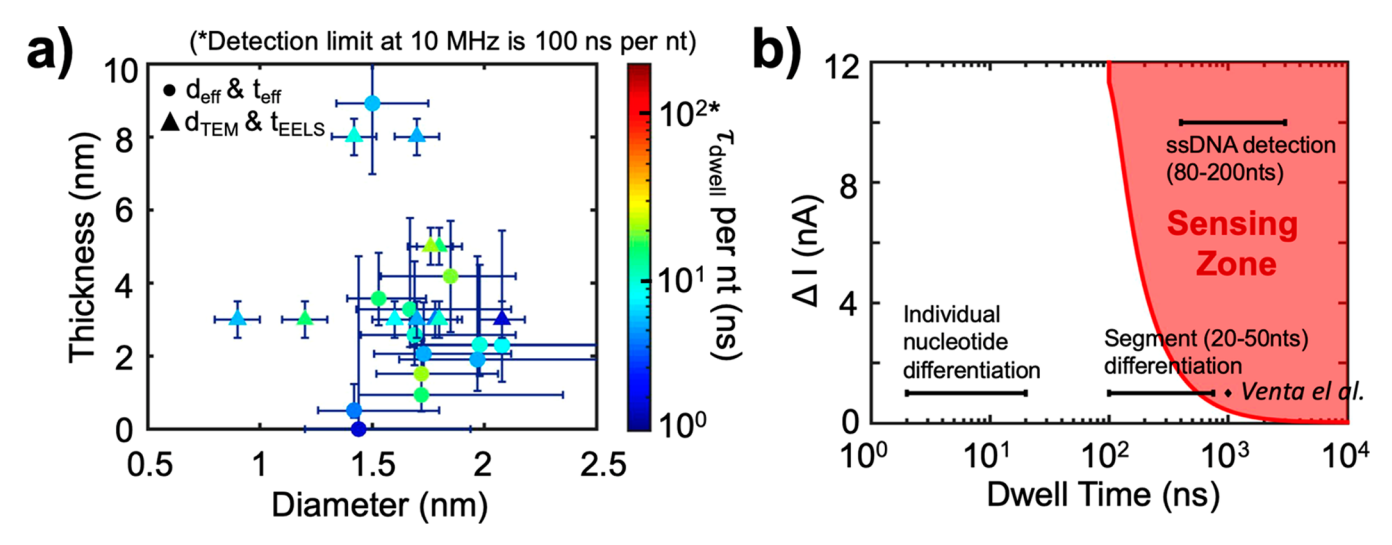


Figure 5. Characteristic dwell times for all pores vs pore diameters and thicknesses and the ssDNA ionic signal, ΔI , vs dwell time, $\tau_{\rm dwell}$ parameter space. (a) Characteristic dwell time per nucleotide ($\tau_{\rm dwell}$ per nt) plotted as a function of the nanopore diameter and thickness for all pores. $d_{\rm eff}$ and $t_{\rm eff}$ are marked as circles, and $d_{\rm TEM}$ and $t_{\rm EELS}$ are marked as triangles in the graph. The time detection limit of a 10 MHz amplifier is 100 ns per nt, above which our 10 MHz amplifier could accurately report a signal from each nucleotide. The blue vertical and horizontal lines represent errors in thickness and diameter, described in the text. DNA used are 90–200 nt long ssDNA, salt solutions are 1 or 3 M KCl, and biased voltages are from 400 to 900 mV, as listed in Table 2. (b) Red curve is the minimum current blockade (ΔI) for translocation events as a function of dwell time to surpass the 5 σ threshold, which we define as the minimum requirement for an event to be detected by the 10 MHz amplifier. Hence, the red area represents the 10 MHz 5 σ "sensing zone". As seen from the red shaded region, for large ΔI , the minimum detection time is 100 ns; as ΔI decreases, the minimum detection time increases to about 500 ns at ΔI = 1 nA. The detection of ssDNA (ΔI = 10 nA, $\tau_{\rm dwell}$ = 0.4–3 μ s), homopolymer segment (20–50 nt) differentiation (ΔI = 1 nA, $\tau_{\rm dwell}$ = 0.1–0.8 μ s), and individual nucleotide differentiation (ΔI = 1 nA, $\tau_{\rm dwell}$ = 2–20 ns) are marked as black horizontal line segments on the graph, and only the right end of the "segment (20–50 nt) differentiation" line overlaps with the "sensing zone". The ΔI from Venta et al. For 30 nt long ssDNA homopolymers with similar pores is marked as the diamond on the graph for reference.

speeds measured in this study, we plot the characteristic dwell time per nucleotide, τ_{dwell} /nt (characteristic dwell time for the molecule divided by the number of nucleotides), as a function of $t_{\rm eff}$ and $d_{\rm eff}$ for the pores used in this study in Figure 5a. Here, we assume a constant DNA speed to estimate the dwell time per nucleotide, and we record $\tau_{\text{dwell}}/\text{nt}$ between 2 and 21 ns/nt across the pores studied, which is 5-50 times shorter than what is resolvable at 10 MHz bandwidth. The shaded red area in Figure 5c, marked as the "sensing zone", is the region of ΔI and τ_{dwell} corresponding to events that can be detected with our measurement system. Specifically, for a feature to be detected by the amplifier, its dwell time has to be longer than the minimum temporal resolution determined by the measurement bandwidth, and the signal ΔI should be more than at least 5 times the noise $I_{\text{BASELINE}}^{\text{rms}}$ at the measurement bandwidth.

Several important benchmarks in the $\Delta I - au_{ ext{dwell}}$ parameter space are marked in Figure 5c as "ssDNA detection", "individual nucleotide differentiation", and "segment differentiation". The ssDNA detection requires ΔI on the order of 10 nA at 1 V bias in 1 M KCl and a characteristic τ_{dwell} range from 0.5 to 3 μ s for 80–200 nt ssDNA, as measured, well within the sensing zone of our detector. We observed a difference in the characteristic translocation time of ssDNA molecules that differ in length for pores similar in dimensions. For example, in Pore E and Pore F, $d_{\text{eff}} = 1.7$ nm for both pores, and the thickness, $t_{\rm eff}$, for Pore E is 3.3 nm and for Pore F is 2.6 nm. The molecules used in Pore E are 200 nt ssDNA, and those in Pore F are 90 nt ssDNA. The au_{dwell} for Pore E was 1 μ s and for Pore F was 2 μ s, which scaled roughly with the ssDNA length used in the two experiments (see Table 2). "Individual nucleotide differentiation" requires ΔI on the order

of 1 nA at 1 V bias^{8,9,28} in 1 M KCl as does "segment differentiation" for homopolymer sequences from 20 to 50 nt long. 8,9,28 Individual nucleotide sensing is completely outside the sensing region for detection, but long homopolymer sequences can be detected,⁸ as indicated in Figure 5b. Efforts of slowing down DNA translocation speed, such as reducing temperature or changing salt solutions from KCl to LiCl, have been proposed. Here, we find that these two approaches came at the expense of SNR at a given bandwidth. Experiments with Pore C were conducted at approximately 4 and at 25 °C (room temperature). The characteristic translocation dwell time increased from 0.8 to 1.0 μ s at lower temperature, but ΔI was reduced from 8.5 to 4.3 nA. The translocation dwell time only slightly increased at this lower temperature, but we sacrificed the SNR due to reduced I and ΔI . We also performed experiments with 1 and 3 M LiCl solution. These solutions were previously observed to slow down translocation by a factor of 10 in ~20 nm diameter SiN pores. 17 With the same experimental conditions as in this previous study, but with much smaller diameter nanopores, we did not detect any translocation events. These results are summarized in Section 8 in the Supporting Information. Other methods for slowing down translocation as performed previously may also be beneficial to resolve bases, in combination with the improved high-bandwidth setup. $^{8,9,16-19}$

CONCLUSIONS

In conclusion, we present a nanopore recording system able to record translocation events at 10 MHz bandwidths by combining a custom CMOS amplifier, \sim 1 pF capacitance nanopore chips, and small and thin a-Si/SiO $_x$ pores. We detect events with durations as short as 100 ns. This work establishes

the robustness of ultrathin a-Si pores for ssDNA measurements and the overall consistency between the ionic current data recorded from similar pores in the diameter range of 1-2 nm. We observe intraevent fluctuations and multiple levels within the events and study the variability of current versus time signatures within the events. However, we cannot identify or articulate any characteristic features within events that can be attributed to the repeated DNA homopolymer sequences, such as distinct current levels for repeated poly(dA) and poly(dC). We attribute this to high $R_{\rm access} \sim R_{\rm pore}$ in these devices and to the entropy of ssDNA. To understand and deconvolve these various contributions to the ionic signal in a regime when $d_{\rm eff}$ ~ $t_{\rm eff} \sim 1$ to 2 nm, further modeling and advanced data analysis tools for large data sets are needed. Approaches to reduce this entropy through geometric or electrostatic control will be important to achieve further progress.

METHODS

The low-stress 100 nm thick SiN_x membrane is supported by a 3 mm diameter circular glass (fused-silica) chip with a thickness of 300 $\mu\mathrm{m}$ and a circular window of 20–30 $\mu\mathrm{m}$ in diameter. The SiN_x membrane is thinned down by reactive ion etching and TEM (JEOL 2010F) to a thickness of 3 nm for nanopore drilling. Before experiments, the nanopore chip is cleaned and wetted using a hot piranha solution for 5 min and rinsed by DI water.

The glass chip is secured with Kwik-cast, a silicone layer that we apply around the SiN membrane to separate electrolyte solutions and as an additional insulating layer that reduces capacitance, on PDMS cells and is separated into two chambers containing a salt solution composed of 1 or 3 M KCl buffered to pH 8 using 10 mM Tris-HCl with 1 mM EDTA. Bias voltages between 0 and 900 mV are applied across the nanopore through Ag/AgCl electrodes. Experiments are carried out using a custom CMOS-integrated nanopore amplifier8 to apply a voltage bias and measure the current through the nanopore simultaneously. The data are recorded using a custom-designed data acquisition board and software at 40 MSps and filtered using a digital approximation of a four-pole low-pass Bessel filter. The output of the amplifier is subjected to boosting filters to restore flat frequency response up until 10 MHz.8 Single-stranded DNA of specific segments and lengths indicated are ordered from IDT (Integrated DNA Technologies, Inc.) and made into stock solution of 20 μ M and stored in the freezer. In each DNA translocation experiments, 200 nM of ssDNA in desired salt solution is made, and 1 μ L of solution is added to the cis chamber of the PDMS cell. Data analysis is done in custommade programs in Matlab (MathWorks, Natick, MA, USA).

ASSOCIATED CONTENT

S Supporting Information

The Supporting Information is available free of charge on the ACS Publications website at DOI: 10.1021/acsnano.9b04626.

Additional information on more experimental details, data on event dwell times, wavelet analysis of translocation events, and event structures and fluctuations and their analysis in the translocation experiments (PDF)

AUTHOR INFORMATION

Corresponding Author

*E-mail: drndic@physics.upenn.edu.

ORCID ®

Siddharth Shekar: 0000-0002-9466-1402 Marija Drndić: 0000-0002-8104-2231

Present Address

¹D.J.N.: Goeppert LLC, Pennovation Works, 3401 Grays Ferry Avenue, Philadelphia, Pennsylvania 19146, United States

Author Contributions

C.-C.C. and S.S. contributed equally to this work. All authors designed the experiments; C.-C.C. and D.J.N. made glass chips and nanopores; C.-C.C., S.S., and D.J.N. performed translocation measurements; C.-C.C. and S.S. analyzed the ionic current data. All authors contributed in the discussion and writing of the manuscript.

Notes

The authors declare the following competing financial interest(s): M.D. is a founder and consultant of Goeppert (www.gppert.com) that manufactures nanotechnology-related products including nanopore chips, fluid cells, and TEM supplies. K.L.S. is a principal in Chimera Instruments, LLC, which is commercializing high-bandwidth voltage-clamp amplifiers.

ACKNOWLEDGMENTS

This work was supported in part by a grant from the W.M. Keck Foundation, by the National Institutes of Health under Grant No. R01HG009189, and by the National Science Foundation under Grant No. EFRI-1542707. Some fabrication work was performed at the University of Pennsylvania's Singh Center for Nanotechnology, an NNCI member supported by NSF Grant ECCS-1542153. M.D., C.-C.C., and D.J.N. also acknowledge use of TEM facilities and instrumentation supported by the NSF through the University of Pennsylvania Materials Research Science and Engineering Center (DMR-1720530). We thank A. Nicolai and W. Parkin for useful comments and discussions.

REFERENCES

- (1) Branton, D.; Deamer, D. W.; Marziali, A.; Bayley, H.; Benner, S. A.; Butler, T.; Di Ventra, M.; Garaj, S.; Hibbs, A.; Huang, X.; Jovanovich, S. B.; Krstic, P. S.; Lindsay, S.; Ling, X. S.; Mastrangelo, C. H.; Meller, A.; Oliver, J. S.; Pershin, Y. V.; Ramsey, J. M.; Riehn, R.; et al. The Potential and Challenges of Nanopore Sequencing. *Nat. Biotechnol.* **2008**, *26*, 1146–1153.
- (2) Derrington, I. M.; Butler, T. Z.; Collins, M. D.; Manrao, E.; Pavlenok, M.; Niederweis, M.; Gundlach, J. H. Nanopore DNA Sequencing with MspA. *Proc. Natl. Acad. Sci. U. S. A.* **2010**, *107*, 16060–16065.
- (3) Clarke, J.; Wu, H.-C.; Jayasinghe, L.; Patel, A.; Reid, S.; Bayley, H. Continuous Base Identification for Single-Molecule Nanopore DNA Sequencing. *Nat. Nanotechnol.* **2009**, *4*, 265–270.
- (4) Jain, M.; Koren, S.; Miga, K. H.; Quick, J.; Rand, A. C.; Sasani, T. A.; Tyson, J. R.; Beggs, A. D.; Dilthey, A. T.; Fiddes, I. T.; Malla, S.; Marriott, H.; Nieto, T.; O'Grady, J.; Olsen, H. E.; Pedersen, B. S.; Rhie, A.; Richardson, H.; Quinlan, A. R.; Snutch, T. P.; et al. Nanopore Sequencing and Assembly of a Human Genome with Ultra-Long Reads. *Nat. Biotechnol.* **2018**, *36*, 338–345.
- (5) Laszlo, A. H.; Derrington, I. M.; Ross, B. C.; Brinkerhoff, H.; Adey, A.; Nova, I. C.; Craig, J. M.; Langford, K. W.; Samson, J. M.; Daza, R.; Doering, K.; Shendure, J.; Gundlach, J. H. Decoding Long Nanopore Sequencing Reads of Natural DNA. *Nat. Biotechnol.* **2014**, 32, 829–834.
- (6) Rosenstein, J. K.; Wanunu, M.; Merchant, C.; Drndić, M.; Shepard, K. L. Integrated Nanopore Sensing Platform with Sub-Microsecond Temporal Resolution. *Nat. Methods* **2012**, *9*, 487–492. (7) Shekar, S.; Niedzwiecki, D. J.; Chien, C.-C.; Ong, P.; Fleischer, D. A.; Lin, J.; Rosenstein, J. K.; Drndić, M.; Shepard, K. L. Measurement of DNA Translocation Dynamics in a Solid-State

Nanopore at 100 ns Temporal Resolution. Nano Lett. 2016, 16, 4483-4489.

- (8) Venta, K.; Shemer, G.; Puster, M.; Rodríguez-Manzo, J. A.; Balan, A.; Rosenstein, J. K.; Shepard, K.; Drndić, M. Differentiation of Short, Single-Stranded DNA Homopolymers in Solid-State Nanopores. *ACS Nano* **2013**, *7*, 4629–4636.
- (9) Feng, J.; Liu, K.; Bulushev, R. D.; Khlybov, S.; Dumcenco, D.; Kis, A.; Radenovic, A. Identification of Single Nucleotides in MoS2 Nanopores. *Nat. Nanotechnol.* **2015**, *10*, 1070–1076.
- (10) Danda, G.; Masih Das, P.; Chou, Y.-C.; Mlack, J. T.; Parkin, W. M.; Naylor, C. H.; Fujisawa, K.; Zhang, T.; Fulton, L. B.; Terrones, M.; Johnson, A. T. C.; Drndic, M. Monolayer WS2 Nanopores for DNA Translocation with Light-Adjustable Sizes. *ACS Nano* **2017**, *11*, 1937–1945.
- (11) Fischbein, M. D.; Drndic, M. Electron Beam Nanosculpting of Suspended Graphene Sheets. *Appl. Phys. Lett.* **2008**, *93*, 113107.
- (12) Garaj, S.; Hubbard, W.; Reina, A.; Kong, J.; Branton, D.; Golovchenko, J. Graphene as a Subnanometre Trans-Electrode Membrane. *Nature* **2010**, *467*, 190–193.
- (13) Merchant, C. A.; Healy, K.; Wanunu, M.; Ray, V.; Peterman, N.; Bartel, J.; Fischbein, M. D.; Venta, K.; Luo, Z.; Johnson, A. C.; Drndic, M. DNA Translocation Through Graphene Nanopores. *Nano Lett.* **2010**, *10*, 2915–2921.
- (14) Schneider, G. F.; Kowalczyk, S. W.; Calado, V. E.; Pandraud, G.; Zandbergen, H. W.; Vandersypen, L. M.; Dekker, C. DNA Translocation Through Graphene Nanopores. *Nano Lett.* **2010**, *10*, 3163–3167.
- (15) Danda, G.; Drndić, M. Two-Dimensional Nanopores and Nanoporous Membranes for Ion and Molecule Transport. *Curr. Opin. Biotechnol.* **2019**, *55*, 124–133.
- (16) Kowalczyk, S. W.; Wells, D. B.; Aksimentiev, A.; Dekker, C. Slowing Down DNA Translocation Through a Nanopore in Lithium Chloride. *Nano Lett.* **2012**, *12*, 1038–1044.
- (17) Wanunu, M.; Sutin, J.; McNally, B.; Chow, A.; Meller, A. DNA Translocation Governed by Interactions with Solid-state Nanopores. *Biophys. J.* **2008**, *95*, 4716–4725.
- (18) Plesa, C.; van Loo, N.; Dekker, C. DNA Nanopore Translocation in Glutamate Solutions. *Nanoscale* **2015**, *7*, 13605.
- (19) Fologea, D.; Uplinger, J.; Thomas, B.; McNabb, D. S.; Li, J. Slowing DNA Translocation in a Solid-State Nanopore. *Nano Lett.* **2005**, *5*, 1734–1737.
- (20) Balan, A.; Machielse, B.; Niedzwiecki, D.; Lin, J.; Ong, P.; Engelke, R.; Shepard, K. L.; Drndic, M. Improving Signal-to-Noise Performance for Dna Translocation in Solid-state Nanopores at MHz Bandwidths. *Nano Lett.* **2014**, *14*, 7215–7220.
- (21) Balan, A.; Chien, C.-C.; Engelke, R.; Drndic, M. Suspended Solid-state Membranes on Glass Chips with sub 1-pF Capacitance for Biomolecule Sensing Applications. *Sci. Rep.* **2016**, *5*, 17775.
- (22) Lee, M.-H.; Kumar, A.; Park, K.-B.; Cho, S.-Y.; Kim, H.-M.; Lim, M.-C.; Kim, Y.-R.; Kim, K.-B. A Low-noise Solid-state Nanopore Platform Based on a Highly Insulating Substrate. *Sci. Rep.* **2015**, *4*, 7448.
- (23) Balan, A.; Drndic, M. Ultra Low Capacitance Glass Supported Dielectric Membranes for Macromolecular Analysis. US Patent Appl. 10,274,478, 2019.
- (24) Rodríguez-Manzo, J. A.; Puster, M.; Nicolaï, A.; Meunier, V.; Drndic, M. DNA Translocation in Nanometer Thick Silicon Nanopores. *ACS Nano* **2015**, *9*, 6555–6564.
- (25) Rosenstein, J. K.; Shepard, K. L. Temporal Resolution of Nanopore Sensor Recordings. *Proc. Annu. Int. Conf. IEEE Eng. Med. Biol. Soc. EMBS* **2013**, 4110–4113.
- (26) Kowalczyk, S. W.; Grosberg, A. Y.; Rabin, Y.; Dekker, C. Modeling the Conductance and DNA Blockade of Solid-state Nanopores. *Nanotechnology* **2011**, *22*, 315101.
- (27) Shekar, S.; Chien, C.-C.; Hartel, A.; Ong, P.; Clarke, O. B.; Marks, A.; Drndic, M.; Shepard, K. L. Wavelet Denoising of High-Bandwidth Nanopore and Ion-Channel Signals. *Nano Lett.* **2019**, *19*, 1090–1097.

- (28) Goto, Y.; Yanagi, I.; Matsui, K.; Yokoi, T.; Takeda, K. Identification of Four Single-stranded DNA Homopolymers with a Solid-state Nanopore in Alkaline CsCl Solution. *Nanoscale* **2018**, *10*, 20844–20850.
- (29) Yamazaki, H.; Hu, R.; Zhao, Q.; Wanunu, M. Photothermally Assisted Thinning of Silicon Nitride Membranes for Ultrathin Asymmetric Nanopores. *ACS Nano* **2018**, *12*, 12472–12481.
- (30) Carlsen, A. T.; Zahid, O. K.; Ruzicka, J.; Taylor, E. W.; Hall, A. R. Interpreting the Conductance Blockades of DNA Translocations Through Solid-State Nanopores. *ACS Nano* **2014**, *8*, 4754–4760.
- (31) Comer, J.; Aksimentiev, A. DNA Sequence-dependent Ionic Currents in Ultra-Small Solid-State Nanopores. *Nanoscale* **2016**, *8*, 9600–9613
- (32) Plumridge, A.; Meisburger, S. P.; Pollack, L. Visualizing Single-Stranded Nucleic Acids in Solution. *Nucleic Acids Res.* **2016**, *45*, No. gkw1297.